



ELSEVIER

Available online at [www.sciencedirect.com](http://www.sciencedirect.com)

 ScienceDirect

Nuclear Physics B (Proc. Suppl.) 175–176 (2008) 155–161

**NUCLEAR PHYSICS B  
PROCEEDINGS  
SUPPLEMENTS**

[www.elsevierphysics.com](http://www.elsevierphysics.com)

## Approaching the Knee with Direct Measurements

E. S. Seo<sup>a,b</sup>, H. S. Ahn<sup>a</sup>, P. Allison<sup>c</sup>, M.G. Bagliesi<sup>d</sup>, L. Barbier<sup>e</sup>, A. Barrau<sup>f</sup>, R. Bazer-Bachi<sup>g</sup>, J. J. Beatty<sup>c</sup>, G. Bigongiari<sup>d</sup>, P. Boyle<sup>h</sup>, T. T. Brandt<sup>c</sup>, M. Buénerd<sup>f</sup>, J. T. Childers<sup>i</sup>, N. B. Conklin<sup>j</sup>, S. Coutu<sup>j</sup>, L. Derome<sup>f</sup>, M. A. DuVernois<sup>i</sup>, O. Ganel<sup>a</sup>, J. H. Han<sup>a</sup>, J. A. Jeon<sup>k</sup>, K. C. Kim<sup>a</sup>, M. H. Lee<sup>a</sup>, L. Lutz<sup>a</sup>, A. Malinin<sup>a</sup>, M. Mangin-Brinet<sup>f</sup>, P. S. Marrocchesi<sup>d</sup>, P. Maestro<sup>d</sup>, A. Menchaca-Rocha<sup>l</sup>, S. Minnick<sup>m</sup>, S. I. Mognet<sup>j</sup>, S. W. Nam<sup>k</sup>, S. Nutter<sup>n</sup>, I. H. Park<sup>k</sup>, N. H. Park<sup>k</sup>, A. Putze<sup>f</sup>, Y. Sallaz-Damaz<sup>f</sup>, R. Sina<sup>a</sup>, S. Swordy<sup>h</sup>, S. Wakely<sup>h</sup>, P. Walpole<sup>a</sup>, J. Wu<sup>a</sup>, J. Yang<sup>k</sup>, Y. S. Yoon<sup>b</sup>, R. Zei<sup>d</sup>, and S. Y. Zinn<sup>a</sup>

<sup>a</sup>*Inst. for Phys. Sci. and Tech., University of Maryland, College Park, MD 20742, USA*

<sup>b</sup>*Dept. of Physics, University of Maryland, College Park, MD 20742, USA*

<sup>c</sup>*Dept. of Physics, Ohio State University, Columbus, Ohio 43210, USA*

<sup>d</sup>*Dept. of Physics, University of Siena and INFN, Via Roma 56, 53100 Siena, Italy*

<sup>e</sup>*NASA Goddard Space Flight Center, Greenbelt, MD 20771, USA*

<sup>f</sup>*Laboratoire de Physique Subatomique et de Cosmologie, Grenoble, France*

<sup>g</sup>*Centre d'Etude Spatiale des Rayonnements, UFR PCA - CNRS - UPR 8002, Toulouse, France*

<sup>h</sup>*Enrico Fermi Institute and Dept. of Physics, University of Chicago, Chicago, IL 60637, USA*

<sup>i</sup>*School of Physics and Astronomy, University of Minnesota, Minneapolis, MN 55455, USA*

<sup>j</sup>*Dept. of Physics, Penn State University, University Park, PA 16802, USA*

<sup>k</sup>*Dept. of Physics, Ewha Womans University, Seoul, 120-750, Republic of Korea*

<sup>l</sup>*Instituto de Fisica, Universidad Nacional Autonoma de Mexico, Mexico*

<sup>m</sup>*Dept. of Physics, Kent State University Tuscarawas, New Philadelphia, OH 44663, USA*

<sup>n</sup>*Dept. of Physics and Geology, Northern Kentucky University, Highland Heights, KY 41099, USA*

The Cosmic Ray Energetics And Mass (CREAM) experiment was designed and constructed to push spectral measurements of individual cosmic-ray nuclei from H to Fe to energies approaching the “knee” in a series of balloon flights. A cumulative exposure of 70 days was achieved during two circumpolar flights in Antarctica in 2005 and 2006. Direct measurements at the top of the atmosphere allow event-by-event determination of the incident cosmic-ray particle charge and energy. The objective is to investigate whether and how the knee structure is related to the mechanisms of particle acceleration, propagation, and confinement. The recovered payload is being refurbished for its third flight, which is scheduled for launch in December 2007. The combination of sophisticated particle detectors and long duration balloon flight capabilities now promise high quality measurements over an energy range that was not previously accessible.

### 1. INTRODUCTION

Shock acceleration is a well accepted explanation for the characteristic power law feature of cosmic-ray energy spectra. However, ground based measurements have shown that the all-particle spectrum extends far beyond the highest energy thought possible for the supernova acceleration theory. The nominal energy for the supernovae acceleration limit is about  $Z \times 10^{14}$  eV,

where  $Z$  is the particle charge [1]. This implies that the all-particles spectrum would be depleted of protons around  $10^{14}$  eV, while heavier nuclei would have correspondingly higher energy limits. The spectrum would be depleted of iron nuclei at 26 times the energy limit for protons. This is nowhere near the maximum energy observed by ground based measurements, but it is intriguingly close the “knee” feature observed by many ground based experiments around  $3 \times 10^{15}$  eV.

A limit to the supernova acceleration process would be reflected by a characteristic change in the elemental composition between the limiting energies for protons and iron, i.e., between  $\sim 10^{14}$  eV and  $2.6 \times 10^{15}$  eV. In other words, protons are the most dominant element at low energies, but heavier elements should become more abundant above the proton acceleration limit  $\sim 10^{14}$  eV, and iron should become most abundant above its nominal acceleration limit around  $2.6 \times 10^{15}$  eV. Note that some theories predict higher maximum energy than  $Z \times 10^{14}$  eV but with the same  $Z$  dependence [2]. The “knee” structure could also be related to energy dependent leakage effects during the propagation process [3,4] or to other effects, such as reacceleration in the galactic wind [5] and acceleration in pulsars [6].

Several ground-based and space-based investigations were initiated to look for evidence of a limit to supernova acceleration in the cosmic-ray chemical composition at high energies approaching the “knee.” Ground level observations of air showers, which can be used to determine the energies of incident cosmic rays without direct charge determination of the particle that initiated the shower, depend heavily on hadronic interaction models and Monte Carlo simulations. Direct measurements at the top of the atmosphere can determine individual elemental spectra and, thereby, test the supernova acceleration model. However, direct measurements in the energy range of interest are technically challenging. The detectors must be large enough to collect adequate statistics, yet light enough to be flown.

Magnet spectrometers such as BESS [7], AMS [8], and Pamela [9] can provide precise measurements of elemental spectra, but their energy reach does not approach the “knee.” The low-density materials needed to fabricate Transition Radiation (TR) detectors make this technique particularly suitable for the large area detectors needed to observe heavy nuclei and rare nuclear species, but its inherent response characteristics are not practical for measuring p and He. The only practical method for energy measurement of all nuclei, including p and He, is calorimetry. The CREAM instrument employs both techniques to extend the elemental spectral measurements to the energies capable of generating air showers, which have mainly been observed on the ground with

indirect measurements. It will have enough overlap with ground based measurements to provide calibration for indirect measurements. Our goal is to explore a limit to the acceleration of cosmic rays in supernova by measuring elemental spectra from protons to Fe nuclei, including secondaries produced in the interactions of primary cosmic rays with the interstellar medium during their propagation in the Galaxy. Simultaneous measurements of secondary and primary nuclei allow the determination of the source spectra at energies where measurements are not currently available.

## 2. THE CREAM EXPERIMENT

The CREAM instrument consists of complementary and redundant particle detectors to measure the charge and energy of ultrahigh energy particles. As shown in Fig. 1, they include a Timing Charge Detector (TCD), a Transition Radiation Detector (TRD) with a Cherenkov Detector (CD), and a calorimeter module

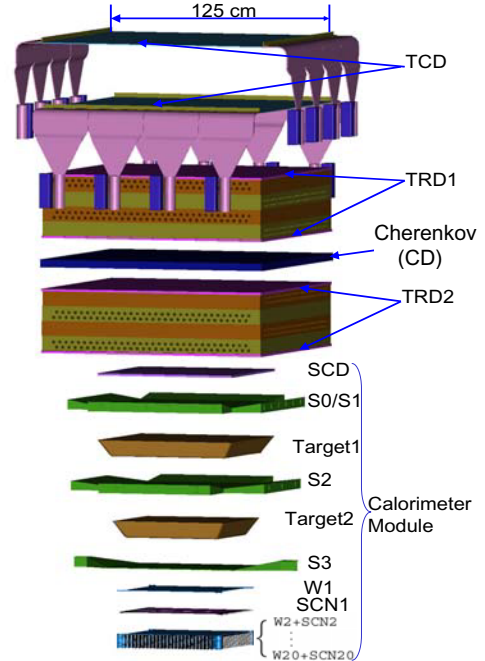


Figure 1. Schematic of the CREAM instrument.

comprised of a Silicon Charge Detector (SCD), a carbon target, scintillating fiber hodoscopes (S0/S1 and S2), and a stack of tungsten plates with interleaved scintillating fiber layers. See reference [10] for the instrument details. A key feature of the instrument is its ability to obtain simultaneous measurements of the energy by the complementary calorimeter and TRD techniques, thereby allowing in-flight inter-calibration for better determination of their energy scales. Multiple charge measurements with the TCD, CD, SCD, and S0/S1 layers of scintillating fibers minimize the effect of backscattered particles from the calorimeter, thereby allowing accurate identification of the incident particle charges.

The TCD measures the incident particle charge based on the fact that the incident particle enters the TCD before developing a shower in the calorimeter, while the backscattered particles arrive several nanoseconds later [11]. A layer of scintillating fibers, S3, located between the carbon target and the tungsten calorimeter provides a reference time. The SCD is segmented into  $2.12 \text{ cm}^2$  pixels to minimize multiple hits of backscattered particles in a segment.

The TRD determines the Lorentz factor for  $Z > 3$  nuclei by measuring transition x-rays using thin-wall gas tubes [12]. Transition radiation is produced when a relativistic particle traverses an inhomogeneous medium, in particular the boundary between materials of different dielectric properties. The TRD consists of the foam radiator and 16 layers of proportional tubes filled with a mixture of Xenon (95 %) and Methane (5%) gas. The Cherenkov Detector (CD) between the two TRD sections provide low energy particle rejection at the flight site, Antarctica, where the geomagnetic cutoff is low. It also provides additional charge identification.

The carbon target forces hadronic interactions in the calorimeter module, which measures the shower energy and provides tracking information to determine which segment(s) of the charge detectors to use for the charge measurement [13]. The shower is sampled each radiation length in the tungsten calorimeter, which has a vertical depth of 20 radiation lengths. The 1 cm wide and 0.5 mm thick scintillating fiber ribbons measure the longitudinal and lateral distributions of the shower. Tracking for showers is accomplished by extrapolating each shower axis back to the charge

detectors. The hodoscopes S0/S1 and S2, comprised of 2 mm thick and 2 mm wide scintillating fibers, provide additional tracking information above the tungsten stack. The tracking uncertainty is smaller than the pixel size of the SCD [14].

Tracking for non-interacting particles is achieved in the TRD with better accuracy (1 mm resolution with 67 cm lever arm, 0.0015 radians). The TRD and calorimeter have different systematic biases in determining particle energy. The use of both instruments allows in-flight cross-calibration of the two techniques and, consequently, provides a powerful method for measuring cosmic-ray energies. The trigger aperture of CREAM is  $\sim 2.2 \text{ m}^2\text{sr}$ , and the highly segmented detectors comprising the instrument have about 10,000 electronic channels.

The instrument was calibrated in a series of beam tests at the CERN SPS, where the highest energy particles are available [15,16,17,18]. As shown in Fig. 2, the beam test data show good agreement with the simulations. Above the available accelerator beam energy, Monte Carlo simulations [14], as shown in Fig. 3, indicate that the calorimeter response is quite linear in the CREAM measurement energy range. Simulations also indicate that the calorimeter energy resolution is nearly energy independent, as shown in Fig. 4.

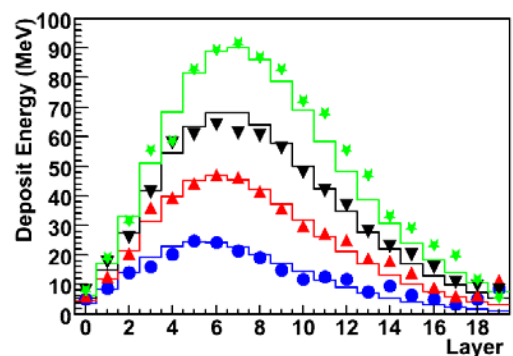


Figure 2. Longitudinal shower profiles for electrons with 50 (blue circles), 100 (red upward triangles), 150 (black downward triangles) and 200 (green star symbol) GeV energies are compared with the Monte Carlo simulations (curves for 50, 100, 150 and 200 GeV from the bottom to top).

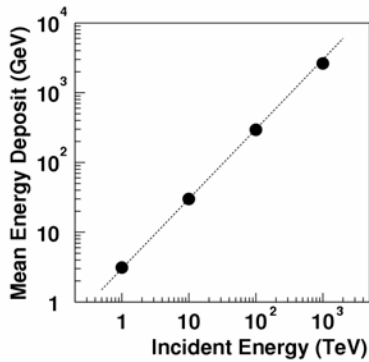


Figure 3. Monte Carlo simulations. Mean energy deposit in the calorimeter as a function of the incident energy.

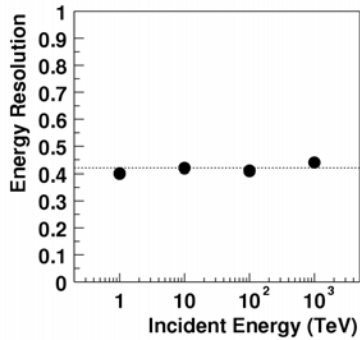


Figure 4. Monte Carlo simulations. The energy resolution, width (1 sigma) of the energy deposit distribution, as a function of the incident energy.

### 3. BALLOON FLIGHTS

The CREAM instrument was designed and constructed to meet the challenging requirements of nominal 100-day ultra long duration balloon flights. It has had two successful flights with a conventional balloon launched from McMurdo, Antarctica [19,20,21]. A conventional balloon launched during the austral summer from McMurdo travels in the polar wind vortex, which carries it around the South Pole, thereby providing a long exposure. The CREAM payload circumnavigated the South Pole three times in a record breaking 42 days from 16 December 2004 to 27 January 2005 during its first flight. It achieved two circumpolar navigations in 28 days from 16 December 2005 to 13 January 2006 during its second flight. In both cases, the

payload was recovered in excellent condition after flying successfully.

The balloon float altitude was between 38 and 40 km throughout most of both flights. The corresponding average atmospheric overburden was  $\sim 3.9 \text{ g/cm}^2$ . The diurnal altitude variation due to the Sun angle change was small,  $< 1 \text{ km}$ , near the Pole, i.e., at high latitude, although it increased slightly as the balloon spiraled outward to lower latitudes later in the flights. The temperature of the various instrument boxes stayed within the required operational range with daily variation of a few  $^\circ\text{C}$ , consistent with the Sun angle. See Reference [22] for more details of the flight operations.

All of the high energy data ( $> \sim 1 \text{ TeV}$ ) were transmitted via the Tracking and Data Relay Satellite System (TDRSS) during the flight, while the lower energy data were recorded on board. A total of 117 GB of data including  $\sim 6.7 \times 10^7$  science events were collected from the two flights. The performance of the instruments flown on the first two flights can be found elsewhere: Calorimeter performance [23, 24], SCD performance [25], TCD/TRD performance [26].

### 4. DATA ANALYSIS

The main trigger conditions for science events were (1) significant energy deposit in the Calorimeter for high energy particles or (2) large pulse height in the TCD for heavy nuclei. Figure 5 shows a preliminary result of the calorimeter energy deposit distribution for events triggered with the condition (1), i.e., the high energy trigger. The red line represents data from Flight-1 and the black line represents cumulative data from Flight-1 and Flight-2. The roll off at low energies is due to the instrumental threshold. Above 3.7 along the horizontal scale, i.e.,  $\sim 10^{3.7} \text{ MeV}$  deposit corresponding to  $\sim 3 \text{ TeV}$  incident energy, the spectrum follows a reasonable power law and the data extend well above 100 TeV incident energy.

Charge measurements are made by extrapolating the reconstructed shower axis to the charge detectors. A preliminary charge distribution from the SCD for energies below 10 TeV, 10 – 50 TeV, and above 50 TeV are compared in Fig. 6a, 6b, and 6c respectively. The

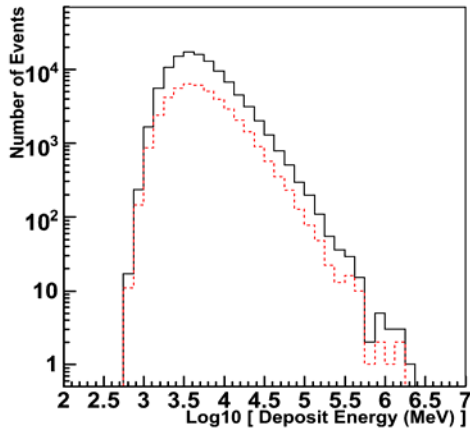


Figure 5. Preliminary energy deposit distribution in the calorimeter for Flight-1 (red dashed line,) and cumulative counts for Flight 1 and 2 (black solid line).

corresponding mean logarithmic mass,  $1.44 \pm 0.02$ ,  $1.64 \pm 0.04$  and  $1.9 \pm 0.2$ , respectively, indicate heavier composition approaching the “knee”. The energy scale is still preliminary, and corrections for background and efficiencies need to be made. Note that the quoted uncertainties are only statistical. Nevertheless, our preliminary result is consistent with previous measurements [27]. Possible causes of the increase in the mean mass include (1) steeper source spectrum for protons than for heavies, (2) preferential loss of high energy protons due to the acceleration limit, (3) flattening of heavy nuclei spectra due to weaker energy dependence in the escape length, (4) artifact due to backscatter, leakage, or some other instrument effect, etc. Further analysis including event reconstruction algorithm development to handle backscattered particles as well as corner-clipping, side entering, and side exiting events is underway, and the related systematic uncertainties are being assessed.

According to the TCD/TRD analysis reported in Reference [28], preliminary spectra of Carbon and Oxygen nuclei from  $\sim 10$  GeV to  $\sim 3 \times 10$  TeV are in good agreement with the HEAO and CRN satellite measurements. Higher energy data are being analyzed. Other preliminary results can be found in [21].

It should be noted that CREAM was afloat and taking data during the large January 20, 2005, solar flare [29]. While the calorimeter and TRD were not

designed to measure the low energies of solar flare particles, and the instrument was not triggered by these low energy particles, they were recorded during periodic pedestal runs of the SCD and hodoscopes. As shown in Figure 7, a sudden increase in readout levels during pedestal runs of the SCD, and hodoscopes S0, S1, and S2 coincided

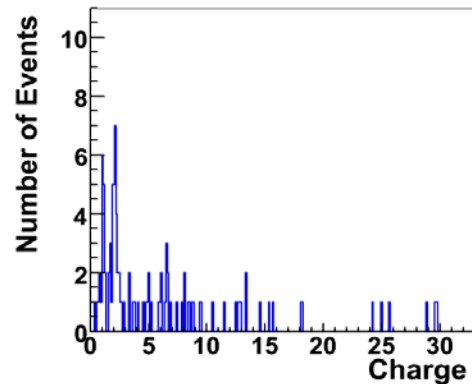
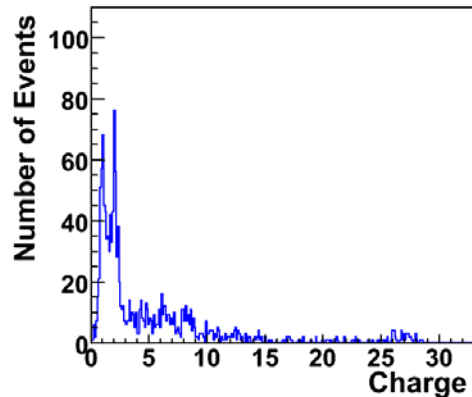
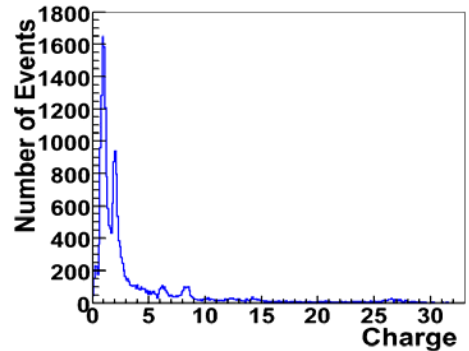


Figure 6. Preliminary SCD charge distribution for energies (a) 3 - 10 TeV, (b) 10 - 50 TeV, and (c) above 50 TeV.

with the reported powerful solar flare and the spike in the GOES-11 proton flux [30]. The counts decrease with depth in the instrument, consistent with an energy spectrum that decreases with increasing energy of the incident particles. Further analysis is underway to explore the highest energy solar energetic particles.

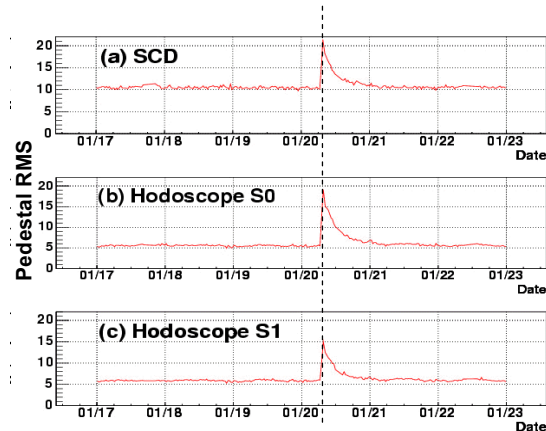


Figure 7. Sudden increase in readout levels during pedestal runs occurred at about 7 am on Jan 20 (GMT) coinciding with a reported powerful solar flare.

## 5. STATUS SUMMARY

With excellent particle charge resolution, two complementary energy measurements, and relatively large collection power, CREAM will extend direct measurements of cosmic ray composition to higher energies approaching the “knee”. In addition, unprecedented solar flare data may allow us to explore the acceleration limit of our Sun.

Further refinements of the calibration, event reconstruction and analysis of data from two flights, and preparation for next flight, are underway. A new addition to the CREAM instrument for Flight-3 is a Cherenkov imager (CherCam) optimized for charge measurements. The CherCam [31] consists of a silica aerogel Cherenkov radiator plane and a photon detector plane with an array of 1600 1-inch diameter photomultiplier tubes. Since the backscatter particles from the calorimeter will be absorbed in the radiator, the CherCam will provide

efficient discrimination against backscatter particles. With CherCam, in addition to the TCD based on timing, and the SCD based on pixellation, the CREAM experiment implements virtually all possible techniques to minimize the backscatter effect on charge measurements in the presence of the calorimeter. Consequently, it is expected to achieve charge measurements with the highest possible accuracy.

## ACKNOWLEDGEMENTS

This work is supported by NASA grants in the U.S., by the Korean Ministry of Science and Technology in Korea, by INFN in Italy, and by IN2P3 in France. The authors thank the NASA Wallops Flight Facility, Columbia Scientific Balloon Facility, National Science Foundation Office of Polar Programs, and Raytheon Polar Service Company for the successful balloon launches, flight operations, and payload recoveries.

## REFERENCES

1. P.O. Lagage and C.J. Cesarsky, *Astron. & Astrophys.* 118 (1983) 223.
2. A.M. Hillas, *J. Phys. G: Nucl. Part. Phys.* 31 (2005) R95.
3. V.S. Ptuskin et al., *Astron. & Astrophys.* 268 (1993) 726.
4. S.P. Swordy, *Proc. 24<sup>th</sup> Int. Cosmic ray Conf., Rome, 2* (1995) 697.
5. H.J. Völk and V.N. Zirakashvili, *Proc. 28<sup>th</sup> Int. Cosmic ray Conf., Tsukuba, 4* (2003) 2031.
6. W. Bednarek and R.J. Protheroe, *Astropart. Phys.* 16 (2002) 397.
7. T. Sanuki et al., *Astrophys. J.* 545 (2000) 1135.
8. M. Aguilar et al., *Phys. Rep.* 366/6 (2002) 331.
9. M. Boenio et al., *Astrophys. J.* 518 (1999) 457.
10. E.S. Seo et al., *Adv. in Space Res.*, 33/10 (2004) 1777;  
<http://cosmicray.umd.edu/cream/cream.html>.
11. J.J. Beatty et al., *Proc. SPIE* 4858 (2003) 248.
12. P.J. Boyle et al., *Proc. 28<sup>th</sup> Int. Cosmic ray Conf., Tsukuba* (2003) 2233.
13. E.S. Seo et al., *Proc. SPIE* 2806 (1996) 134.

14. H.S. Ahn et al., Proc. 27th Int. Cosmic Ray Conf., Hamburg, 6 (2001) 2159.
15. Y.S. Yoon et al., Proc. 29th Int. Cosmic Ray Conf., Pune, 8 (2005) 371.
16. I.H. Park et al., Nucl. Instrum. Meth. A535 (2004) 158.
17. P.S. Marrocchesi et al., Proc. 29th Int. Cosmic Ray Conf., Pune, 3 (2005) 309.
18. H.S. Ahn et al., Proc. 11th Int. Conf. on Calorimetry in Part. Phys. - CALOR2004, Perugia, Italy (2004) 532.
19. E.S. Seo et al., Proc. 29th Int. Cosmic Ray Conf., Pune, 3 (2005) 101.
20. E.S. Seo et al., Proc. 29th Int. Cosmic Ray Conf., Pune, 10 (2005) 185.
21. E.S. Seo et al., Adv. in Space Res. (2006) in press.
22. Y.S. Yoon et al., Proc. 29th Int. Cosmic Ray Conf., Pune, 3 (2005) 429.
23. M.H. Lee et al., Proc. 29th Int. Cosmic Ray Conf., Pune, 3 (2005) 417.
24. P.S. Marrocchesi et al., Adv. in Space Res. (2006) in press.
25. N. H. Park et al., J. of Korean Phys. Soc. 49, No. 2 (2006) 815.
26. S. Coutu et al., Proc. 29th Int. Cosmic Ray Conf., Pune, 3 (2005) 393.
27. J. R. Hörandel, astro-ph/ 0508014 (2005).
28. S.P. Wakely et al., Adv. in Space Res. (2006) in press.
29. R.A. Mewaldt et al., Proc. 29th Int. Cosmic Ray Conf., Pune, 1 (2005) 111.
30. [http://www.sec.noaa.gov/ftpd/ftpdir/plots/2005\\_plots/proton/20050121\\_proton.gif](http://www.sec.noaa.gov/ftpd/ftpdir/plots/2005_plots/proton/20050121_proton.gif)
31. M. Buenerd et al., Proc. 29th Int. Cosmic Ray Conf., Pune, 3 (2005) 277.